DOI: 10.1002/chem.200800776

Two-Dimensionally Extended Porphyrin Tapes: Synthesis and Shape-Dependent Two-Photon Absorption Properties

Yasuyuki Nakamura,[a] So Young Jang,[b] Takayuki Tanaka,[a] Naoki Aratani,[a] Jong Min Lim,[b] Kil Suk Kim,[b] Dongho Kim,*[b] and Atsuhiro Osuka*[a]

Abstract: We report the synthesis and characterization of L- and T-shaped porphyrin tapes as extensible structural motifs of two-dimensionally extended porphyrin tapes. The two-photon absorption (TPA) cross-section values ($\sigma^{(2)}$) for L- and T-shaped porphyrin tapes as well as those for linear trimeric and tetrameric porphyrin tapes were measured by an open-aperture Z-scan method at 2300 nm, a wavelength at which the one-photon absorption contribution is either zero or almost negligible. Under these conditions, the $\sigma^{(2)}$ values for the linear porphyrin tape trimer and tetramer were determined to be 18500 and 41200 GM, respectively. The $\sigma^{(2)}$ value for the L-shaped trimer was determined to be 8700 GM, which is only half that of the linear trimer, whereas the $\sigma^{(2)}$ value for the T-shaped tetramer was measured to be 35700 GM. These results clearly indicate the dependence of the TPA cross-section on the molecular shape, which underscores the importance of directionality in the π-conjugation pathway for the enhancement of TPA cross-section.

Keywords: aromaticity · conjugation · nonlinear optics · porphyrinoids · two-photon adsorption

Introduction

Two-photon absorption (TPA) is one of the nonlinear optical (NLO) phenomena in which a chromophore is excited by simultaneous absorption of two low-energy photons to a level at which normal high-energy one-photon absorption is required. This TPA property can be linked to numerous potential applications, for example, 3D microfabrication,[1,2] optical storage,[3,4] optical-limiting devices,[5,6] and photodynamic therapy.[7] Hence, extensive studies have been carried out to elucidate the molecular structure–property relationships for TPA. From these studies it has been concluded that extended π-electron conjugation and large molecular polarizability are the key factors that contribute to a large TPA cross-section.[8–22] Recent efforts have been directed towards enhancing this TPA property by using donor(D)/acceptor(A)-type multichromophore systems with a D–π–A arrangement,[11] introducing additional groups to perturb the charge redistribution, and elongating the effective π-conjugation length.[18] Alternatively, intramolecular face-to-face π-conjugated systems lead to large $\sigma^{(2)}$ values as a result of favorable cofacial π electronic interactions.[19] Dendrimers[20] and expanded porphyrins[21] have also been shown to be promising molecular platforms for large TPA properties. Octupolar effects have also been reported to be advantageous for large TPA cross-section values.[22] Despite these extensive studies, the effects of structure on this TPA property are not clearly understood.

Porphyrin has been shown to be a very versatile pigment that gives large TPA properties by appropriate chemical modification.[23–31] Although porphyrin monomers usually exhibit only small TPA cross-sections (<100 GM),[23] this TPA property has been enhanced by effective conjugation.[24–31] In this respect, *meso–meso*,β–β,β–β triply linked porphyrin arrays (porphyrin tapes)[32–35] are particularly promising because the arrays are fully conjugated electronic systems, as seen in their extremely redshifted absorption bands. They are also interesting in light of their flat and rigid molecular shapes,[32] their ability to store multiple

[a] Y. Nakamura, T. Tanaka, Dr. N. Aratani, Prof. Dr. A. Osuka
Department of Chemistry, Graduate School of Science
Kyoto University
Sakyo-ku, Kyoto 606-8502 (Japan)
Fax: (+81) 75-753-3970
E-mail: osuka@kuchem.kyoto-u.ac.jp

[b] S. Y. Jang, J. M. Lim, K. S. Kim, Prof. Dr. D. Kim
Center for Ultrafast Optical Characteristics Control and
Department of Chemistry
Yonsei University, Seoul 120-749 (Korea)
Fax: (+82) 2-2123-2434
E-mail: dongho@yonsei.ac.kr

Supporting information for this article is available on the WWW under http://dx.doi.org/10.1002/chem.200800776.

charges,[33] and their electronically communicative guest binding.[34] In fact, the TPA cross-section values ($\sigma^{(2)}$) of dimer **2**, trimer **3**, and tetramer **4** have been revealed to be exceptionally large, 11900, 33100, and 93600 GM, respectively, in an open aperture Z-scan measurement using femtosecond laser pulse excitation at 1200 nm (Scheme 1).[36] However, note that the large TPA values for **3** and **4** contain non-negligible contributions from the one-photon absorption at 1200 nm. Thus, it is highly desirable to measure TPA values free from the contribution of the one-photon absorption by shifting the two-photon excitation wavelength further into the IR region in which porphyrin arrays do not absorb.

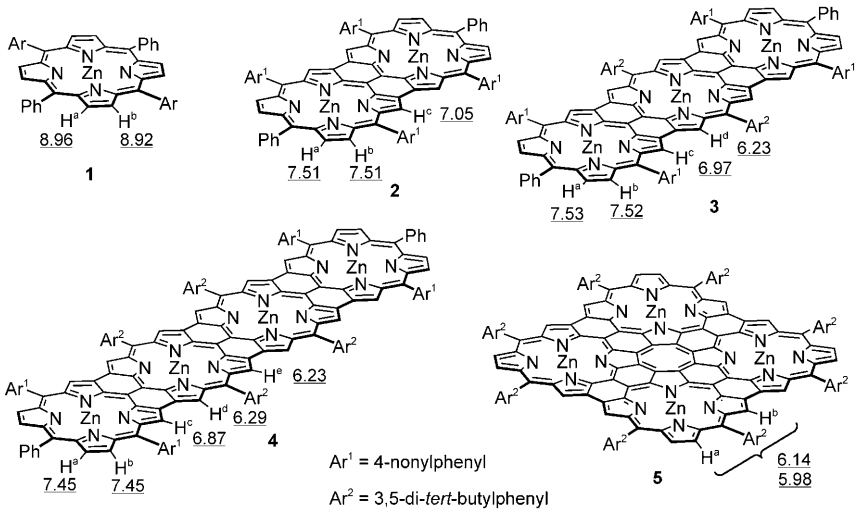

Scheme 1. Structures of porphyrin **1** and porphyrin arrays **2**–**5**. The ^{1}H NMR chemical shifts (δ/ppm) are reported (underlined values).

Triply linked porphyrin tapes are also attractive for a study of the shape-dependence of TPA cross-sections because two-dimensionally extended porphyrin tapes, such as L- and T-shaped arrays, would give the relevant useful information. So far, however, porphyrin tapes have been limited to linear arrays and two-dimensionally extended porphyrin tapelike conjugated porphyrin oligomers have rarely been studied with the exception of tetrameric porphyrin sheet **5**. This square-shaped tetramer exhibits a paratropic ring current above the central cyclooctatetraene (COT) segment and exhibits a small $\sigma^{(2)}$ value of 2750 GM in spite of its tetraporphyrin construction.[37] These results clearly indicate the dependence of the TPA cross-section on the molecular shape and electronic nature of the π-electron system. Consequently, the study of other two-dimensionally extended porphyrin tapelike oligomers is strongly desirable.

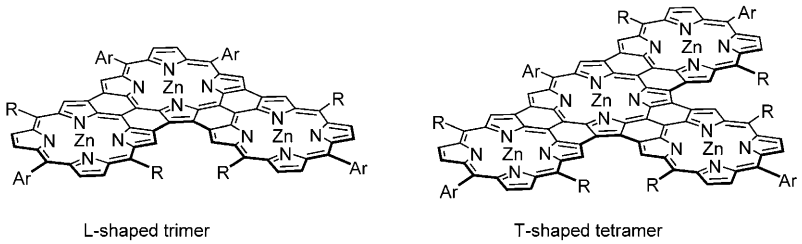

Scheme 2. L- and T-shaped porphyrin tapes studied in this paper.

In this paper, we report the synthesis of L- and T-shaped porphyrin tapes as two-dimensionally extended porphyrin tapes (Scheme 2). The molecular shapes of these porphyrin tapes are interesting from the viewpoint of connectors for direction change or for the multiple connection of a molecular wire in a molecular circuit. We also report the TPA properties of the L- and T-shaped porphyrin tapes as well as those of the linear porphyrin tape trimer **3** and tetramer **4** determined by excitation at 2300 nm, a wavelength at which their real absorptions are zero or almost negligible.[38]

Results

Molecular design and synthesis: L- and T-shaped porphyrin tapes can be regarded as the constructs of a core porphyrin segment (CP) and side-porphyrin segments (SP) (Figure 1).

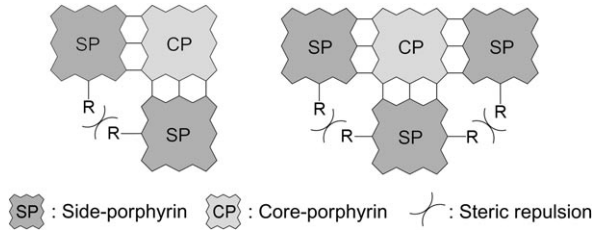

Figure 1. Schematic representation of the structures of the 2D triply linked porphyrin oligomers.

We thus planned to synthesize these molecules by coupling the respective segments and subsequent oxidative ring closure (ORC) to provide L- and T-shaped porphyrin tapes bearing direct triple linkages.[39] In the molecular design of these fused porphyrin arrays, it is important to avoid severe steric interactions between the *meso*-R substituents on the side-porphyrins in the bay area because these substituents

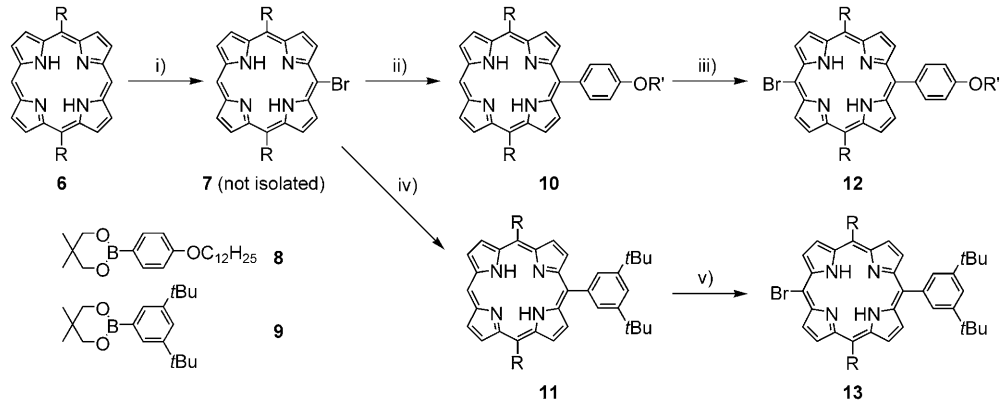

Scheme 3. Synthesis of the side-porphyrins. Reagents: i) NBS, $CHCl_3$; ii) **8**, $[Pd_2(dba)_3{\cdot}CHCl_3]$, PPh_3, K_2CO_3, toluene, DMF; iii) NBS, $CHCl_3$; iv) **9**, $[Pd_2(dba)_3{\cdot}CHCl_3]$, PPh_3, K_2CO_3, toluene, DMF; v) NBS, $CHCl_3$. R = C_9H_{19}, R′ = $C_{12}H_{25}$.

are forced into close proximity (Figure 1). To circumvent these steric interactions, we chose relatively long alkyl substituents for the *meso*-R groups with the expectation that their flexible conformations would help mitigate such interactions and would also help improve their solubility.

Another key issue in the molecular design is to improve the solubility of these porphyrin arrays. Based on our previous studies, *meso–meso* singly linked porphyrin oligomers are expected to have good solubilities,[40–42] but fused porphyrin tapes with flat shapes should display only poor solubilities, which will cause serious difficulties in manipulations and poor reaction yields. This tendency would be worse for two-dimensionally extended L- and T-shaped arrays. Furthermore, the very poor solubility of *meso*-hexahexyl-substituted triply linked diporphyrin warns of seriously poor solubility for L- and T-shaped porphyrin tapes with all-*meso*-alkyl substituents.[43] Accordingly, we decided to employ 5,15-dinonyl-10-(4-dodecyloxyphenyl)porphyrin (**10**) and 5,15-dinonyl-10-(3,5-di-*tert*-butylphenyl)porphyrin (**11**) as SPs and 5,10-bis(3,5-di-*tert*-butylphenyl)porphyrin (**14**)[44] and 5-(3,5-di-*tert*-butylphenyl)porphyrin (**17**)[45] as CPs in the synthesis of the L- and T-shaped porphyrin arrays, respectively (Scheme 3).

5,15-Dinonylporphyrin **6** was synthesized as the starting compound for the synthesis of SP in 19% yield from bis(2-pyrryl)methane and decanal by using the acid-catalyzed condensation method of Lindsey et al.[46] Bromination of **6** with *N*-bromosuccinimide (NBS) and subsequent Suzuki–Miyaura cross-coupling with aryl boronates **8** and **9** gave trisubstituted porphyrins **10** and **11**, respectively. Bromination of **10** and **11** with NBS afforded brominated SPs **12** and **13** in almost quantitative yields.

As synthetic precursors of the CP, multiply borylated porphyrins **16** and **19** were prepared from **14** and **17**, respectively, by a two-step conversion: bromination and borylation (Scheme 4).[47] The bromination yields were 97 and 61% for **15** and **18**, respectively, and the borylation yields were 88 and 64% for **16** and **19**, respectively. Although brominated porphyrins **15** and **18** are only poorly soluble in common organic solvents, borylated porphyrins **16** and **19** exhibit good

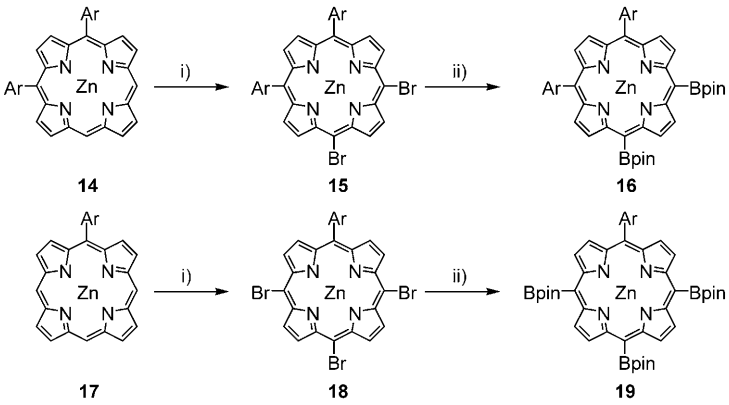

Scheme 4. Synthesis of the core-porphyrins. Reagents: i) NBS, $CHCl_3$; ii) HBpin, $[Pd(PPh_3)_2Cl_2]$, Et_3N, dichloroethane. Ar = 3,5-di-*tert*-butylphenyl, Bpin = 4,4,5,5-tetramethyl-1,3,2-dioxaborolan-2-yl.

solubility and can be easily purified by silica gel column chromatography. In the borylation reaction of **18**, partially debrominated bisborylated porphyrins (1:2 regioisomeric mixture by ^{1}H NMR spectroscopy analysis) were formed as byproducts.

Cross-coupling between CP and SP was performed under Suzuki–Miyaura reaction conditions (Scheme 5).[48] Namely, compounds **16** and **12** (2.2 equiv) were heated at 100 °C in the presence of $[Pd_2(dba)_3{\cdot}CHCl_3]$ (dba = dibenzylideneacetone), PPh_3, Cs_2CO_3, and CsF for 12 h and subsequent separation by GPC–HPLC gave trimer **LHa** in 57% yield. A similar coupling reaction of **19** with **12** (3.3 equiv) afforded tetramer **THa** in 62% yield. *meso–meso* linked oligomers **LHb** and **THb** were similarly obtained by the coupling reaction of **13** with **16** and **19**, respectively, but the yields were only moderate (36% for **LHb** and 20% for **THb**), probably due to the lower solubility of **13**. All-zinc-metalated oligomers **LZa**, **LZb**, **TZa**, and **TZb** were prepared quantitatively by the usual zinc metalation method. The synthesized oligomers were fully characterized by mass spectrometry and ^{1}H NMR spectroscopy (see the Supporting Information).

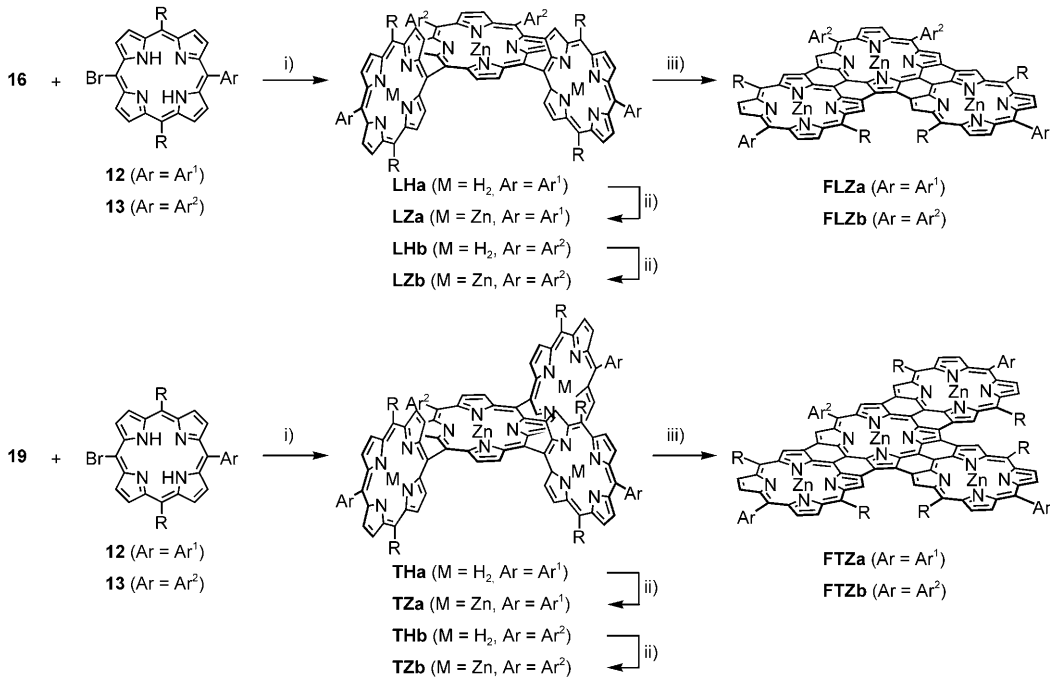

Scheme 5. Synthesis of the L- and T-shaped-porphyrin arrays. Reagents: i) $[Pd_2(dba)_3{\cdot}CHCl_3]$, PPh_3, Cs_2CO_3, CsF, toluene, DMF; ii) $[Zn(OAc)_2{\cdot}2H_2O]$, $CHCl_3$; iii) DDQ, $Sc(OTf)_3$, toluene. R = C_9H_{19}, Ar^1 = 4-dodecyloxyphenyl, Ar^2 = 3,5-di-*tert*-butylphenyl.

Next, the ORC reactions of the L- and T-shaped *meso–meso* linked porphyrin arrays were examined (Scheme 5). Oxidation of **LZa** with 2,3-dichloro-5,6-dicyano-1,4-benzoquinone (DDQ) and $Sc(OTf)_3$ (Tf = trifluoromethanesulfonyl) in toluene[32] and subsequent separation by alumina column chromatography and recrystallization from CH_2Cl_2/CH_3CN gave triply linked L-shaped trimer **FLZa** in a high yield of 89%. A similar ORC reaction of **LZb** gave **FLZb** in 77% yield. The MALDI-TOF mass spectra of the triply linked porphyrin arrays showed the parent ion peaks at *m*/*z* 2511.2 for **FLZa** (calcd for $C_{160}H_{192}N_{12}O_2Zn_3$: 2511.3) and at *m*/*z* 2367.2 for **FLZb** (calcd for $C_{152}H_{176}N_{12}Zn_3$: 2367.2) (see Figure S30 of the Supporting Information). The T-shaped tetramers **FTZa** and **FTZb** were also obtained by the ORC reaction of **TZa** and **TZb** in 85 and 75% yields, respectively. Their mass spectra exhibit the parent ion peaks at *m*/*z* 3203.2 for **FTZa** (calcd for $C_{202}H_{242}N_{16}O_3Zn_4$: 3203.8) and at *m*/*z* 2987.7 for **FTZb** (calcd for $C_{190}H_{218}N_{16}Zn_4$: 2987.5). Comparison of the weak but well-resolved isotope distribution patterns of **TZb** and **FTZb** clearly demonstrates the loss of 12 hydrogen atoms from the corresponding *meso–meso* linked porphyrin array compared with the porphyrin tape (see Figure S32 of the Supporting Information). The GPC chromatograms of the porphyrin tapes **FLZa** and **FTZa** exhibit single peaks under high dilution conditions, and their retention times are slightly but distinctly shorter than those of the corresponding *meso–meso* singly linked porphyrin arrays, which indicates that their hydrodynamic volumes are smaller after the ORC reaction (see Figures S33 and S34 of the Supporting Information).

^{1}H NMR spectra: Porphyrin tapes have conjugated π-electron systems that are extensively delocalized over the whole molecular array. These fully conjugated features are likely to decrease the aromaticity in each porphyrin moiety, as seen in the substantial upfield shifts of the peripheral β protons, which are increasingly eminent for longer porphyrin tapes, as shown in Scheme 1. Namely, the β protons of the porphyrin monomer **1** resonate at $\delta = 8.96$ and 8.92 ppm, which reflects a strong aromatic ring current, and the edge β protons of dimer **2**, trimer **3**, and tetramer **4** resonate at $\delta =$ 7.51, 7.53, and 7.45 ppm, respectively, whereas the inner protons resonate at a higher field.[49] These ^{1}H NMR spectra were recorded in CD_2Cl_2 in the presence of a small amount of *n*-butylamine to suppress the aggregation of the porphyrin tapes by coordination of *n*-butylamine to the zinc ions of the porphyrins. On the other hand, the ^{1}H NMR spectrum of the square planar porphyrin sheet **5** exhibits signals at $\delta =$ 6.14 and 5.98 ppm for the outer β protons.[37] The unique feature of **5** may be ascribed to its central COT segment, which is forced to be planar because of the fused porphyrin skeleton. This structure has been shown to produce a rather strong paratropic ring current just above the COT core, as evidenced by the downfield shifts of the guest protons coordinated to **5**.[37,50]

In this study, we examined the ^{1}H NMR spectra of L- and T-shaped porphyrin tapes in CD_2Cl_2/*n*-butylamine. Even under these conditions, **FLZa** yielded a ^{1}H NMR spectrum with considerably broadened signals, probably due to its strong stacking tendency. This porphyrin tape gives similar broad ^{1}H NMR spectra in $CDCl_3$/*n*-butylamine and

[D_5]pyridine. Fortunately, we found that **FLZb**, which has four bulky 3,5-di-*tert*-butylphenyl substituents, exhibits a sharp ^{1}H NMR spectrum in CD_2Cl_2/*n*-butylamine. Signal assignment was based on comprehensive ^{1}H–^{1}H COSY experiments and by comparison with those of related porphyrins

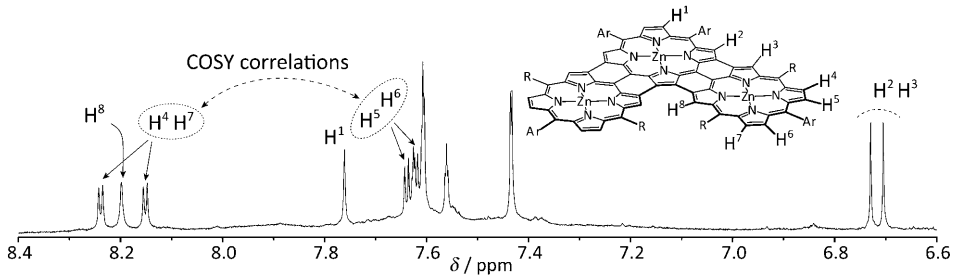

Figure 2. ^{1}H NMR spectrum of **FLZb** in CD_2Cl_2 containing 1% (v/v) *n*-butylamine.

(Figure 2). Three singlet peaks observed at $\delta = 7.76$, 6.73, and 6.71 ppm were assigned to 1-H, and 2-H or 3-H, respectively, because these chemical shifts are similar to those of **3**. The singlet at $\delta = 8.20$ ppm was assigned to 8-H, which is additionally influenced by the ring current of the diagonal porphyrin thereby undergoing a further downfield shift. Two sets of mutually coupled doublet peaks at $\delta = 8.24$ and 8.15 ppm and at $\delta = 7.64$ and 7.63 ppm have been assigned to 4-H or 7-H and 5-H or 6-H, respectively. Overall, the ^{1}H NMR spectrum of **FLZb** indicates that its ring current effect is not so very different to that of **3**, which suggests that the aromaticity of the constituent porphyrins is not strongly perturbed by the L shape of triply linked porphyrin arrays.

The ^{1}H NMR spectra of both **FTZa** and **FTZb** were found to exhibit rather broad signals in the coordinating solvent systems CD_2Cl_2/*n*-butylamine and [D_5]pyridine, even at elevated temperatures, which indicates that the stacking of T-shaped porphyrin tape structures is stronger than that of L-shaped porphyrin tapes.

UV/Vis/NIR absorption spectra: One of the most attractive features of the porphyrin tapes is their unusual absorption spectra that reach into the infrared region as a consequence of full conjugation over the arrays.[51] The absorption spectra of the linear porphyrin tapes are divided into three regions: two higher-energy bands (bands I and II) correspond to a split Soret band and a lower-energy band (band III) that corresponds to the Q band. With an increase in the number of porphyrin units, bands II and III are increasingly redshifted and intense, whereas band I remains at around 410 nm. These spectral changes have been interpreted in terms of a decrease in the HOMO–LUMO gap and decreased molecular symmetry upon elongation of the arrays.[32] In contrast, porphyrin sheet **5** with a highly symmetric square structure exhibits a weak and broad absorption band in the NIR region.[37] These previous studies indicate that the absorption spectra of the conjugated porphyrin tapes are dependent upon molecular shape. In this respect, the absorption spectra of the L- and T-shaped porphyrin tapes are intriguing.

The absorption spectra of **FLZa** and **FTZa** were measured in toluene containing 5% (v/v) *n*-butylamine to suppress aggregation and hence improve their solubility (see Figure 3 and the Supporting Information). However, as judged from the broad ^{1}H NMR spectra, these two porphyrin tapes are considered not to escape aggregation. Without *n*-butylamine, the absorption spectra of **FLZa** in various solvents show a broader structure, which indicates a slight solvent dependency. On the other hand, upon addition of 5% *n*-butylamine, the absorption bands in such solvents become sharpened and redshifted as a consequence of coordination-induced dissociation (see the Supporting Information). The absorption spectrum of **FLZa** can be divided into three major bands, bands I, II, and III in the ranges of 330–680, 700–900, and 1250–1800 nm, which seemingly correspond to bands I, II, and III of the linear porphyrin tapes, respectively. In these three regions, **FLZa** shows band peaks at 499, 788, and 1622 nm, which are almost the same, but slightly redshifted compared with those of the linear trimer **3**. Note, however, that the relative intensities of the three bands are different; the relative intensities of bands II and III of **FLZa** are smaller than those of **3**.

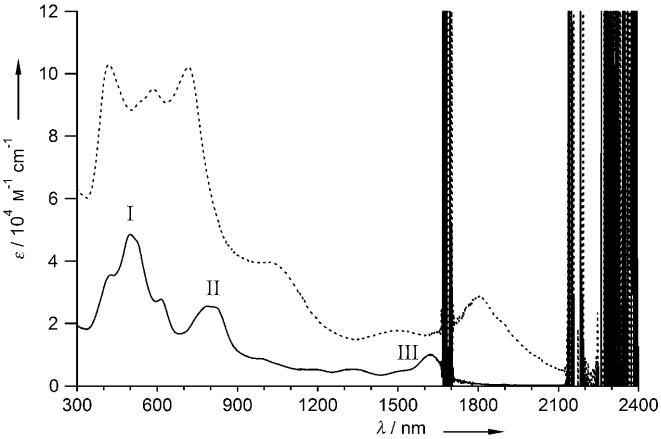

Figure 3. UV/Vis/NIR absorption spectra of **FLZa** (——) and **FTZa** (-----) in toluene containing 5% (v/v) *n*-butylamine.

The absorption spectra of **FTZa** are also dependent upon the solvent and *n*-butylamine (see the Supporting Information). The absorption spectrum of **FTZa** in toluene in the presence of *n*-butylamine shows complicated features with band peaks at 419, 584, 716, 1010, 1504, and 1805 nm (Figure 3). Whereas the peak position of the lowest-energy band is comparable to that of linear tetramer **4** (1813 nm in

$CHCl_3$/*n*-butylamine), the relative intensities of the absorption bands are quite different. The three strong absorption bands at 419, 584, and 716 nm may correspond to band I, whereas the band at 1010 nm and the bands at 1504 and 1805 nm may correspond to bands II and III, respectively. Similarly to **FLZa**, the relative intensity of band III is considerably smaller than that of linear porphyrin tape **4**, probably as a consequence of the bent structure of the porphyrin tape.

TPA properties: The electronic conjugative effects as well as the shape dependence of various *meso–meso*,β–β,β–β triply linked zinc(II) porphyrin arrays are further gleaned from their TPA cross-section ($\sigma^{(2)}$) values, which are largely proportional to the electron-delocalization strength of the molecule. The TPA cross-section values were measured by using an open-aperture Z-scan method by exciting the molecule with IR pulses from an IR optical parametric amplifier pumped by a femtosecond Ti:sapphire regenerative amplifier system with a 130 fs pulse width (Figure 4).

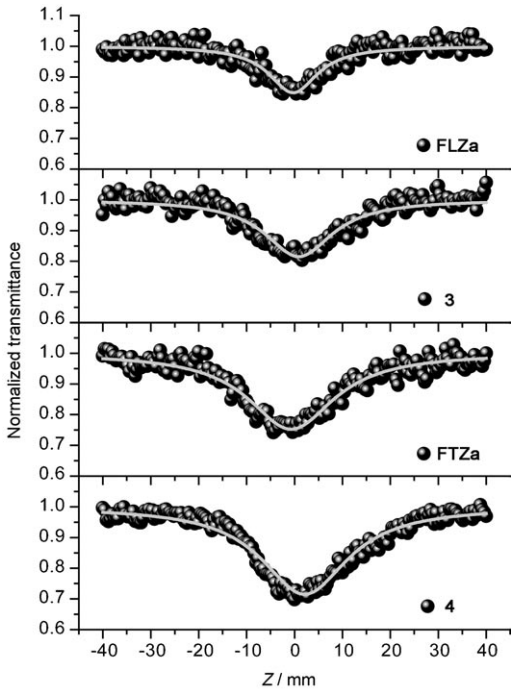

Figure 4. Z-scan curves of **FLZa**, **3**, **FTZa**, and **4** excited at 2300 nm in toluene containing 5% (v/v) *n*-butylamine.

In this study, we chose an excitation wavelength of 2300 nm for the TPA measurements, a wavelength at which the ground-state absorption contribution to the TPA cross-section values is negligible. Note that at 2300 nm there is almost no absorbance for **3** and **4** in $CHCl_3$ containing 5% (v/v) *n*-butylamine in which the TPA experiments were performed. At 2300 nm the $\sigma^{(2)}$ values for **3** and **4** were measured to be 18500 and 41200 GM, respectively. The $\sigma^{(2)}$ values for **FLZa** and **FTZa** were measured to be 9560 and 43000 GM at 2100 nm and 8700 and 35700 GM at 2300 nm, respectively. The $\sigma^{(2)}$ values at 2100 nm were measured to assess the contribution of the small one-photon absorbance especially for **FTZa**.

Discussion

Linear porphyrin tapes **2**, **3**, and **4** exhibit a continuous redshift of the lowest Q-band transition into the infrared region, which indicates that **2**, **3**, and **4** are fully π-conjugated over all the porphyrin planes (see Figure S24 of the Supporting Information). The X-ray structure of **2** shows that the two porphyrin rings are fused to form a coplanar saddle-like conformation with a mean plane deviation of 0.16 Å,[49] which is quite favorable for full π conjugation. However, compounds **2**, **3**, and **4** tend to aggregate due to intrinsically strong π–π stacking. Thus we have employed *n*-butylamine to dissociate aggregates of **2**, **3**, and **4** in solution. The absorption spectra of **2**, **3**, and **4** measured in toluene containing 5% *n*-butylamine exhibit a continuous redshift of the Q-bands (band III) into the IR region in addition to the enhanced exciton-split Soret bands in the 400–800 nm region (bands I and II) (see Figure S24 of the Supporting Information). This indicates that the π-conjugation pathway is elongated throughout the whole molecular framework in **2**, **3**, and **4**. The excited singlet state (π,π*) lifetimes of 4.5, 2.9, and 0.7 ps for **2**, **3**, and **4**, respectively, are also consistent with a continuous decrease in the HOMO–LUMO gaps, which leads to an acceleration of the internal conversion processes from S_1 to S_0 in going from **2** to **3** to **4**.[51] Porphyrin sheet **5** exhibits considerably broadened absorption bands over a wide range, from the UV/Vis to the near-IR regions, which can roughly be divided into three distinct spectral regions: band I (300–600 nm), band II (600–1000 nm), and band III (1000–1500 nm) (see Figure S25 of the Supporting Information).[37] Band III is considerably weaker than that of the one-dimensional tetrameric porphyrin tape **4**. The transient absorption decay profile of **5** reveals a single exponential decay with a time constant of 1.1 ps, which indicates that the lifetime of the S_1 (π,π*) state of **5** is slightly longer than that of tetrameric porphyrin tape **4** (0.72 ps).

The $\sigma^{(2)}$ value for **2** without any contribution from one-photon absorption was measured to be 11900 GM at 1200 nm in our previous work.[36] Because the absorption spectra of **3** and **4** are spread across a wide spectral range down to the IR region, we chose an excitation wavelength of 2300 nm, a wavelength at which the ground-state contributions to the TPA cross-section values should be negligible (Table 1). The $\sigma^{(2)}$ values for **3** and **4** were measured to be 18500 and 41200 GM. But these values are much smaller than the values of 33100 and 93600 GM for **3** and **4**, respectively, measured at 1200 nm in our previous work, which indicates that there was one-photon contribution to the $\sigma^{(2)}$ values. We think that the TPA cross-section value of 41200 GM for **4** is, to the best of our knowledge, the largest

Table 1. TPA cross-section ($\sigma^{(2)}$) values and excitation wavelengths (λ) for fused porphyrin arrays in toluene containing 5% (v/v) *n*-butylamine.

	$\sigma^{(2)}$ [GM]	λ [nm]		$\sigma^{(2)}$ [GM]	λ [nm]
3	20600±1000	2100	**3**	18500±800	2300
			4	41200±1000	2300
FLZa	9560±1000	2100	**FLZa**	8700±800	2300
FTZa	43000±1000	2100	**FTZa**	35700±1000	2300

one without any one-photon contribution ever reported for single chromophore macrocyclic dyes. The hyperpolarizability (β) and $\sigma^{(2)}$ values qualitatively exhibit a linear relationship and they increase with elongation of the π-conjugation length. In this context, the very large $\sigma^{(2)}$ values for **2**, **3**, and **4** observed in this investigation suggest that π-electron delocalization throughout the porphyrin array framework and the completely flat structures are the determining factors that enhance the NLO properties.

In our previous work, the $\sigma^{(2)}$ value for **5** was determined at 1600 nm, a wavelength at which the linear absorption is almost negligible.[37] Despite its tetrameric porphyrin construction, the porphyrin sheet exhibits a very small TPA value of 2750 GM, which is much smaller than that of the corresponding tetrameric porphyrin tape **4**, which suggests that the electronic structure of **5** is quite unique.[37] This indicates that the two-dimensional elongation of the π-conjugation pathway does not guarantee enhanced TPA, which reinforces the belief that molecular polarizability is an important factor in increasing the TPA cross-section values. Note that, based on the NMR experiments, there is a strong paratropic ring current along the COT core that propagates across the whole π network of **5**, affecting the local 18π-electron aromatic porphyrin systems, whereas the four zinc(II) porphyrin subunits still preserve a weak diatropic ring current.[37,50] Thus, the weakening of the overall aromaticity by the central COT core in **5** seems to be responsible for the much reduced TPA cross-section value of **5** compared with the corresponding linear fused array **4**.

To extend our investigation on the shape-dependent TPA properties of porphyrin-fused arrays, we have examined the TPA properties of **FLZa** and **FTZa** in which the constituent porphyrin moieties are connected in L and T shapes. The $\sigma^{(2)}$ value (8700 GM) for **FLZa** is only half that of linear trimer **3**. Note that the $\sigma^{(2)}$ value for **FLZa** is comparable to that of dimer **2**. On the other hand, the $\sigma^{(2)}$ value for **FTZa** was measured to be 35700 GM, which is still smaller than that of the corresponding linear shape tetramer **4**, but distinctly larger than that of the trimer **3**. However, in **FTZa** there is the possibility of a one-photon absorption contribution to the $\sigma^{(2)}$ value due to a very weak absorption tail in the two-photon excitation at a wavelength of 2300 nm.[52] For this reason the $\sigma^{(2)}$ value for **FTZa** may be smaller than that of linear tetramer **4**. Thus, this study clearly suggests that the unidirectional change in the molecular polarizability arising from π-electron delocalization throughout the molecular framework is a key factor in the enhancement of the TPA cross-section values.

Conclusion

L- and T-shaped porphyrin tapes have been prepared through rational synthetic routes and have been fully characterized with a particular focus on their TPA properties in comparison with those of linear porphyrin tapes. The $\sigma^{(2)}$ values for the linear tri- and tetramer porphyrin tapes were measured to be 18500 and 41200 GM, respectively, at an excitation wavelength of 2300 nm. Under similar conditions, the $\sigma^{(2)}$ values for the L-shaped tapes **FLZa** and **FTZa** were measured to be 8700 and 35700 GM. These data clearly substantiate the importance of directionality in the π-conjugation pathway for a large TPA. Thus we believe this work provides benchmark results especially in relation to the origin of the enhancement of TPA cross-section values for π-conjugated porphyrin arrays, which will further help the process of the molecular design of molecules with large TPA properties.

Experimental Section

General procedures: All reagents and solvents were of commercial reagent grade and were used without further purification except where noted. Dry toluene was obtained by distilling over CaH_2. DMF was distilled from K_2CO_3 before use. ^{1}H NMR spectra were recorded on a JEOL ECA-delta-600 spectrometer (600 MHz); chemical shifts (δ) are reported in ppm relative to $CHCl_3$ (δ = 7.26 ppm) or CH_2Cl_2 (δ = 5.30 ppm). Mass spectra were recorded on a Shimadzu/KRATOS KOMPACT MALDI 4 spectrometer using the positive-MALDI ionization method with a 9-nitroanthracene or dithranol matrix or on a Shimadzu/AXIMA-CFR plus spectrometer using the positive-MALDI ionization method with a dithranol matrix. Spectroscopic grade toluene and $CHCl_3$ were used as solvents for all spectroscopic studies. UV/Vis absorption spectra were recorded on a Shimadzu UV-3100 spectrophotometer. Preparative separations were performed by silica gel flash column chromatography (Merck Kieselgel 60H Art. 7736), silica gel gravity column chromatography (Wako gel C-400), and size exclusion gel permeation chromatography (Bio-Rad Bio-Beads S-X1, packed with toluene or $CHCl_3$ in a 4×100 cm gravity flow column). Recycling preparative GPC–HPLC was carried out on a JAI LC-908 instrument using a combination of preparative JAI-GEL-2H and 2.5H columns ($CHCl_3$ as eluent).

5,5-Dimethyl-2-[4-(*p*-dodecyloxy)phenyl]-1,3,2-dioxaborinane (**8**) and 5,5-dimethyl-2-(3,5-di-*tert*-butylphenyl)-1,3,2-dioxaborinane (**9**) were synthesized from *p*-bromododecyloxybenzene and 3,5-di-*tert*-butylbromobenzene, respectively, following a conventional synthetic method.

In the ^{1}H NMR spectra, some of the signals from the nonyl and dodecyl groups were not identified.

Zinc insertion: A saturated solution of $Zn(OAc)_2$ in methanol was added to a solution of the free-base porphyrin in $CHCl_3$ and the resulting mixture was stirred for 2–3 h at ambient temperature (40–50 °C). The reaction mixture was washed with aqueous $NaHCO_3$, then water, and extracted with $CHCl_3$. The organic layer was dried with anhydrous Na_2SO_4, passed through a short plug of silica gel, and evaporated to remove the solvent. Purification was carried out by silica gel column chromatography and recrystallization.

5,15-Dinonylporphyrin (6): Bis(2-pyrrolyl)methane (1.6 g, 11 mmol) and freshly distilled decanal (0.70 mL, 11 mmol) were dissolved in deoxygenated CH_2Cl_2 (2.05 L). After stirring for 10 min under a N_2 atmosphere, trifluoroacetic acid (0.1 equiv) was added to the solution and stirred for 10.5 h at room temperature in the dark. DDQ (3.7 g, 1.5 equiv) was added to the reaction mixture and stirred for 1 h. Then the resulting mixture was passed through an alumina and then a silica gel column. The

purple solution obtained was evaporated to remove the solvent and the residue was purified by recrystallization from CH_2Cl_2/CH_3CN (0.60 g, 19%). ^1H NMR ($CDCl_3$): $\delta = 10.16$ (s, 2H; *meso*-H), 9.57 (d, $J = 4.6$ Hz, 4H; β-H), 9.41 (d, $J = 4.6$ Hz, 4H; β-H), 5.01 (t, $J = 8.0$ Hz, 4H; C_9H_{19}-α), 2.55 (m, 4H; C_9H_{19}-β), 1.81 (m, 4H; C_9H_{19}-γ), 1.53 (m, 4H; C_9H_{19}-δ), 0.88 (t, $J = 7.1$ Hz, 6H; C_9H_{19}-Me), 2.91 ppm (s, 2H; NH); MS (MALDI-TOF): *m/z*: calcd for $C_{38}H_{50}N_4$: 562.8; found: 561.6.

5,15-Dinonyl-10-(*p*-dodecyloxyphenyl)porphyrin (10): NBS (47 mg, 0.26 mmol) was added to a solution of **6** (250 mg, 0.44 mmol) in $CHCl_3$ purged with N_2 (for 15 min) and the solution was stirred for 10 min under a N_2 atmosphere at 0°C in the dark. The reaction mixture was poured into water and extracted with $CHCl_3$. The organic layer was washed with brine and water, dried with anhydrous Na_2SO_4, and then evaporated to remove the solvent. The purple residue, compound **8** (260 mg, 1.8 equiv), [$Pd_2(dba)_3$·$CHCl_3$] (21 mg, 6 mol%), PPh_3 (25 mg, 24 mol%), and K_2CO_3 (230 mg, 1.8 equiv) were dissolved in a mixture of toluene (1.5 mL) and DMF (1.0 mL). The solution was deoxygenated through freeze–pump–thaw cycles and the resulting solution was heated at 85°C for 15 h under an argon atmosphere. After cooling, the reaction mixture was washed with water and extracted with $CHCl_3$. The organic layer was dried with anhydrous Na_2SO_4, passed through a short plug of silica gel, and evaporated to remove the solvent. The product was purified by silica gel column chromatography (CH_2Cl_2/hexane) and recycling preparative GPC–HPLC (91 mg, 42% from **6**). ^1H NMR ($CDCl_3$): $\delta = 10.04$ (s, 1H; *meso*-H), 9.54 (d, $J = 4.7$ Hz, 2H; β-H), 9.43 (d, $J = 4.7$ Hz, 2H; β-H), 9.34 (d, $J = 4.7$ Hz, 2H; β-H), 8.93 (d, $J = 4.7$ Hz, 2H; β-H), 8.09 (d, $J = 8.0$ Hz, 2H; Ar-H), 7.27 (d, $J = 8.0$ Hz, 2H; Ar-H), 4.97 (t, $J = 8.2$ Hz, 4H; C_9H_{19}-α), 4.27 (t, $J = 6.6$ Hz, 4H; $C_{12}H_{25}$-α), 2.53 (m, 4H; C_9H_{19}-β), 2.02 (m, 4H; $C_{12}H_{25}$-β), 1.79 (m, 4H; C_9H_{19}-γ), 1.65 (m, 4H; $C_{12}H_{25}$-γ), −2.84 ppm (s, 2H; NH); MS (MALDI-TOF): *m/z*: calcd for $C_{56}H_{78}N_4O$: 823.2; found: 823.8.

5,15-Dinonyl-10-(*p*-dodecyloxyphenyl)-20-bromoporphyrin (12): NBS (21 mg, 1.2 equiv) was added to a solution of **10** (85 mg, 0.10 mmol) in $CHCl_3$ purged with N_2 (for 15 min) and the solution was stirred for 15 min under a N_2 atmosphere at 0°C in the dark. The reaction mixture was added to water and extracted with $CHCl_3$. The organic layer was washed with brine and water, dried with anhydrous Na_2SO_4, and then evaporated to remove the solvent. The residue was purified by silica gel column chromatography ($CHCl_3$/hexane). Yield: 88 mg, 95%; ^1H NMR ($CDCl_3$): $\delta = 9.73$ (d, $J = 4.6$ Hz, 2H; β-H), 9.47 (d, $J = 4.8$ Hz, 2H; β-H), 9.36 (d, $J = 4.8$ Hz, 2H; β-H), 8.85 (d, $J = 4.6$ Hz, 2H; β-H), 8.04 (d, $J = 6.4$ Hz, 2H; Ar-H), 7.28 (d, $J = 6.4$ Hz, 2H; Ar-H), 4.91 (t, $J = 8.1$ Hz, 4H; C_9H_{19}-α), 4.27 (t, $J = 6.4$ Hz, 2H; $C_{12}H_{25}$-α), 2.49 (m, 4H; C_9H_{19}-β), 2.00 (m, 2H; $C_{12}H_{25}$-β), 1.77 (m, 4H; C_9H_{19}-γ), 1.64 (m, 2H; $C_{12}H_{25}$-γ), 1.50 (m, 4H; C_9H_{19}-δ), 1.43 (m, 2H; $C_{12}H_{25}$-δ), 0.91 (t, $J = 7.1$ Hz, 3H; $C_{12}H_{25}$-Me), 0.87 (t, $J = 7.0$ Hz, 6H; C_9H_{19}-Me), −2.66 ppm (s, 2H; NH); MS (MALDI-TOF): *m/z*: calcd for $C_{56}H_{77}BrN_4O$: 902.1; found: 901.9.

5,15-Dinonyl-10-(3,5-di-*tert*-butylphenyl)porphyrin (11): This porphyrin was prepared from **7** and **9** using the procedure as that used for the preparation of **10**. Yield: 93 mg, 30%; ^1H NMR ($CDCl_3$): $\delta = 10.05$ (s, 1H; *meso*-H), 9.55 (d, $J = 4.1$ Hz, 2H; β-H), 9.43 (d, $J = 4.6$ Hz, 2H; β-H), 9.35 (d, $J = 5.0$ Hz, 2H; β-H), 8.91 (d, $J = 4.6$ Hz, 2H; β-H), 8.04 (s, 2H; Ar-H), 7.81 (s, 1H; Ar-H), 4.98 (t, $J = 8.7$ Hz, 4H; C_9H_{19}-α), 2.55 (m, 4H; C_9H_{19}-β), 1.52 (s, 18H; *t*Bu), 0.85 (t, $J = 6.9$ Hz, 6H; C_9H_{19}-Me), −2.82 ppm (s, 2H; NH); MS (MALDI-TOF): *m/z*: calcd for $C_{52}H_{70}N_4$: 751.1; found: 901.9.

5,15-Dinonyl-10-(3,5-di-*tert*-butylphenyl)-20-bromoporphyrin (13): NBS (11 mg, 1.2 equiv) was added to a solution of **11** (39 mg, 0.052 mmol) in $CHCl_3$ purged with N_2 (for 15 min) and the solution was stirred for 15 min under a N_2 atmosphere at 0°C in the dark. The reaction mixture was added to water and extracted with $CHCl_3$. The organic layer was washed with brine and water, dried with anhydrous Na_2SO_4, and then evaporated to remove the solvent. The residue was purified by silica gel column chromatography ($CHCl_3$/hexane). Yield: 41 mg, 95%, 0.049 mmol; ^1H NMR ($CDCl_3$): $\delta = 9.72$ (d, $J = 4.8$ Hz, 2H; β-H), 9.47 (d, $J = 4.6$ Hz, 2H; β-H), 9.36 (d, $J = 4.1$ Hz, 2H; β-H), 8.85 (d, $J = 4.6$ Hz, 2H; β-H), 8.01 (s, 2H; Ar-H), 7.81 (s, 1H; Ar-H), 4.91 (t, $J = 7.8$ Hz, 4H; C_9H_{19}-α), 2.51 (m, 4H; C_9H_{19}-β), 1.52 (s, 18H; *t*Bu), 0.87 (t, $J = 7.1$ Hz, 6H; C_9H_{19}-Me), −2.65 ppm (s, 2H; NH); MS (MALDI-TOF): *m/z*: calcd for $C_{52}H_{69}BrN_4$ 830.0; found: 831.0.

[5,10-Bis(3,5-di-*tert*-butylphenyl)-15,20-dibromoporphyrinato]zinc(II) (15): NBS (100 mg, 2.1 equiv) was added to a solution of **14** (200 mg, 0.27 mmol) in $CHCl_3$ purged with N_2 (for 15 min) and a drop of pyridine, and the solution was stirred for 3 min under a N_2 atmosphere at 0°C in the dark. The reaction mixture was added to water and extracted with $CHCl_3$. The organic layer was washed with brine and water, dried with anhydrous Na_2SO_4, and then evaporated to remove the solvent. The residue was purified by silica gel column chromatography ($CHCl_3$/hexane). Yield: 235 mg, 0.26 mmol, 97%; ^1H NMR ($CDCl_3$): $\delta = 9.64$ (d, $J = 4.7$ Hz, 2H; β-H), 9.53 (s, 2H; β-H), 8.97 (d, $J = 4.7$ Hz, 2H; β-H), 8.94 (s, 2H; β-H), 8.05 (s, 4H; Ar-H), 7.81 (s, 2H; Ar-H), 1.55 ppm (s, 36H; *t*Bu); MS (MALDI-TOF): *m/z*: calcd for $C_{48}H_{50}Br_2N_4Zn$ 908.2; found: 907.5; UV/Vis ($CHCl_3$): $\lambda_{max} = 606$, 565, 428 nm.

[5,10-Bis(3,5-di-*tert*-butylphenyl)-15,20-bis(4,4,5,5-tetramethyl-1,3,2-dioxaborolan-2-yl)porphyrinato]zinc(II) (16): Triethylamine (0.98 mL, 26 equiv) was added with a syringe to a solution of **15** (235 mg, 0.26 mmol), 4,4,5,5-tetramethyl-1,3,2-dioxaborolane (0.62 mL, 16 equiv), and [$Pd(PPh_3)_2Cl_2$] (19 mg, 10 mol%) in dry 1,2-dichloroethane (20 mL) purged with argon (for 15 min) and the solution was stirred for 2 h at reflux under an argon atmosphere. The resulting mixture was passed through a short plug of silica gel with CH_2Cl_2 as eluent and purified by silica gel column chromatography (CH_2Cl_2/hexane). The first band was **14** (231 mg, 0.23 mmol, 88%), the second band was 5,10-bis(3,5-di-*tert*-butylphenyl)-15-(4,4,5,5-tetramethyl-1,3,2-dioxaborolan-2-ylporphyrinato)zinc(II), and the third was **16**. ^1H NMR ($CDCl_3$): $\delta = 10.05$ (s, 2H; β-H), 9.87 (d, $J = 4.6$ Hz, 2H; β-H), 9.11 (d, $J = 4.6$ Hz, 2H; β-H), 9.00 (s, 2H; β-H), 8.06 (s, 4H; Ar-H), 7.79 (s, 2H; Ar-H), 1.88 (s, 24H; Bpin), 1.52 ppm (s, 36H; *t*Bu); UV/Vis ($CHCl_3$): $\lambda_{max} = 550$, 421 nm; MS (MALDI-TOF): *m/z*: calcd for $C_{60}H_{74}B_2N_4O_4Zn$: 1002.3; found: 1002.3.

[5-(3,5-Di-*tert*-butylphenyl)-10,15,20-tribromoporphyrinato]zinc(II) (18): NBS (21 mg, 3.3 equiv) was added to a solution of **17** (20 mg, 36 μmol) in $CHCl_3$ purged with N_2 (for 15 min) and a drop of pyridine, and the solution was stirred for 10 min under a N_2 atmosphere at 0°C in the dark. The reaction mixture was added to water and extracted with $CHCl_3$. The organic layer was washed with brine and water, dried with anhydrous Na_2SO_4, and then evaporated to remove the solvent. The residue was purified by silica gel column chromatography ($CHCl_3$/hexane). Yield: 17.4 mg, 22 μmol, 61%; ^1H NMR ($CDCl_3$): $\delta = 9.66$ (m, 4H; β-H), 9.62 (d, $J = 4.6$ Hz, 2H; β-H), 8.94 (d, $J = 4.4$ Hz, 2H; β-H), 8.01 (s, 2H; Ar-H), 7.84 (s, 1H; Ar); UV/Vis ($CHCl_3$): $\lambda_{max} = 611$, 569, 430 nm; MS (MALDI-TOF): *m/z*: calcd for $C_{34}H_{29}Br_3N_4Zn$: 798.7; found: 798.3.

[5-(3,5-Di-*tert*-butylphenyl)-10,15,20-tris(4,4,5,5-tetramethyl-1,3,2-dioxaborolan-2-yl)porphyrinato]zinc(II) (19): Triethylamine (0.83 mL, 39 equiv) was added with a syringe to a solution of **18** (112 mg, 0.15 mmol), 4,4,5,5-tetramethyl-1,3,2-dioxaborolane (0.52 mL, 24 equiv), and [$Pd(PPh_3)_2Cl_2$] (10 mg, 10 mol%) in dry 1,2-dichloroethane (10 mL) purged with argon (for 15 min), and the solution was stirred for 1.5 h at steady reflux under an argon atmosphere. The resulting mixture was passed through a short plug of silica gel with CH_2Cl_2 and purified by silica gel column chromatography (Et_2O/hexane). The first fraction was **17**, the second was monoborylated porphyrin, the third was bis-borylated porphyrin, and the forth was **19** (91 mg, 0.097 mmol, 64%). ^1H NMR ($CDCl_3$): $\delta = 10.08$ (d, $J = 4.7$ Hz, 2H; β-H), 10.50 (d, $J = 4.7$ Hz, 2H; β-H), 9.91 (d, $J = 4.7$ Hz, 2H; β-H), 9.14 (d, $J = 4.7$ Hz, 2H; β-H), 8.08 (d, $J = 1.8$ Hz, 2H; Ar), 7.83 ppm (t, $J = 1.7$ Hz, 1H; Ar); UV/Vis ($CHCl_3$): $\lambda_{max} = 585$, 550, 418 nm; MS (MALDI-TOF): *m/z*: calcd for $C_{52}H_{65}B_3N_4O_6Zn$: 939.9; found: 939.3.

Typical procedure for the palladium-catalyzed Suzuki–Miyaura cross-coupling reactions: The borylated porphyrin **16** or **19** (1.0 equiv), the brominated porphyrin **12** or **13** (2.2 equiv for the L-shaped array, 3.3 equiv for the T-shaped array), [$Pd_2(dba)_3$·$CHCl_3$] (5 mol% versus brominated porphyrin), PPh_3 (20 mol% versus brominated porphyrin), Cs_2CO_3 (2.0 equiv versus brominated porphyrin), and CsF (1.5 equiv versus brominated porphyrin) were dissolved in a mixture of toluene and DMF (2:3). The solution was deoxygenated by freeze–pump–thaw cycles and

the resulting solution was heated at 100 °C for 12 h under an argon atmosphere. After cooling, the reaction mixture was poured into water and extracted with $CHCl_3$. The organic layer was dried with anhydrous Na_2SO_4, passed through a short plug of silica gel, and evaporated to remove the solvent. The product was purified by recycling preparative GPC–HPLC. Insertion of zinc(II) into the isolated compounds by using $[Zn(OAc)_2{\cdot}2H_2O]$ gave the all-zinc-metalated compounds.

LHa: Yield: 57%; ^{1}H NMR ($CDCl_3$): δ = 9.40 (d, J = 4.3 Hz, 4H; β-H), 9.17 (d, J = 4.3 Hz, 4H; β-H), 9.14 (s, 2H; β-H), 8.92 (d, J = 4.3 Hz, 4H; β-H), 8.81 (d, J = 4.8 Hz, 2H; β-H), 8.22–8.19 (m, 12H), 8.13 (d, J = 8.2 Hz, 2H; *o*-Ar-H), 8.07 (d, J = 8.2 Hz, 2H; *o*-Ar-H), 7.87 (s, 2H; β-H), 7.76 (s, 2H; β-H), 4.88 (brs, 8H; C_9H_{19}-α), 4.27 (t, J = 6.2 Hz, 4H; $C_{12}H_{25}$-α), 2.47 (m, 8H; C_9H_{19}-β), −2.16 ppm (s, 4H; NH) (*m*-Ar-H signals were obscured by the $CHCl_3$ peak); UV/Vis ($CHCl_3$): $\lambda_{max}(\varepsilon)$ = 658 (12600), 599 (21600), 561 (66300), 523 (58100), 457 (294000), 412 nm (233000 $M^{-1}cm^{-1}$); MS (MALDI-TOF): *m*/*z*: calcd for $C_{160}H_{204}N_{12}O_2Zn$: 2392.8; found: 2391.3.

LZa: Yield: quant; ^{1}H NMR ($CDCl_3$): δ = 9.52 (d, J = 4.8 Hz, 4H; β-H), 9.29 (d, J = 4.8 Hz, 4H; β-H), 9.15 (s, 2H; β-H), 9.02 (d, J = 4.9 Hz, 4H; β-H), 8.79 (d, J = 4.6 Hz, 2H; β-H), 8.13 (d, J = 4.8 Hz, 4H; β-H), 8.20 (d, J = 1.9 Hz, 4H; *o*-Ar-H), 8.16 (d, J = 4.6 Hz, 2H; β-H), 8.14 (dd, J = 9.4 Hz, J = 2.2 Hz, 2H; *o*-Ar-H), 8.07 (dd, J = 8.4 Hz, J = 2.2 Hz, 2H; *o*-Ar-H), 7.81 (s, 2H; β-H), 7.75 (t, J = 1.9 Hz, 2H; *p*-Ar-H), 7.30 (dd, J = 8.4 Hz, J = 2.6 Hz, 2H; *m*-Ar-H), 7.26 (dd, J = 8.0 Hz, J = 2.6 Hz, 2H; *m*-Ar-H), 4.93 (t, J = 7.3 Hz, 8H; C_9H_{19}-α), 4.27 (t, J = 6.7 Hz, 4H; $C_{12}H_{25}$-α), 2.52 (m, 8H; C_9H_{19}-β), 2.00 (m, 4H; $C_{12}H_{25}$-β), 1.77 (m, 8H; C_9H_{19}-γ), 1.64 $C_{12}H_{25}$-γ), 1.50 (s, 36H; *t*Bu), 0.90 (t, J = 7.1 Hz, 6H; $C_{12}H_{25}$-Me), 0.78 ppm (t, J = 6.9 Hz, 12H; C_9H_{19}-Me); UV/Vis ($CHCl_3$): $\lambda_{max}(\varepsilon)$ = 566 (60300), 461 (261000), 414 nm (213000 $M^{-1}cm^{-1}$); MS (MALDI-TOF): calcd for $C_{160}H_{200}N_{12}O_2Zn_3$: 2519.4; found: 2519.2.

LHb: Yield: 22%; ^{1}H NMR ($CDCl_3$): δ = 9.42 (d, J = 4.8 Hz, 4H; β-H), 9.19 (d, J = 4.3 Hz, 4H; β-H), 9.16 (s, 2H; β-H), 8.92 (d, J = 4.8 Hz, 2H; β-H), 8.83 (d, J = 4.6 Hz, 2H; β-H), 8.23 (d, J = 4.6 Hz, 4H; β-H), 8.21 (d, J = 1.9 Hz, 4H; *o*-Ar-H), 8.09 (t, J = 1.6 Hz, 2H; *o*-Ar-H), 8.04 (t, J = 1.6 Hz, 2H; *o*-Ar-H), 7.91 (s, 2H; β-H), 7.82 (t, J = 1.7 Hz, 2H; *p*-Ar-H), 7.77 (t, J = 1.7 Hz, 2H; *p*-Ar-H), 4.89 (t, J = 7.9 Hz, 8H; C_9H_{19}-α), 2.49 (m, 8H; C_9H_{19}-β), 1.75 (m, 8H; C_9H_{19}-γ), 1.57 (s, 18H; *t*Bu), 1.53 (s, 18H; *t*Bu), 1.52 (s, 36H; *t*Bu), 0.79 (t, J = 6.3 Hz, 12H; C_9H_{19}-Me), −2.12 ppm (brs, 4H; NH); MS (MALDI-TOF): *m*/*z*: calcd for $C_{152}H_{188}N_{12}Zn$: 2248.6; found: 2249.5.

LZb: Yield: quant; ^{1}H NMR ($CDCl_3$): δ = 9.54 (d, J = 4.8 Hz, 4H; β-H), 9.30 (d, J = 4.8 Hz, 4H; β-H), 9.16 (s, 2H; β-H), 9.03 (d, J = 4.8 Hz, 4H; β-H), 8.81 (d, J = 4.6 Hz, 2H; β-H), 8.33 (d, J = 4.8 Hz, 4H; β-H), 8.21 (s,4H; *o*-Ar-H), 8.19 (d, J = 4.8 Hz, 2H; β-H), 8.11 (s, 2H; *o*-Ar-H), 8.04 (s, 2H; *o*-Ar-H), 7.83 (s, 2H; β-H), 7.81 (s, 2H; *p*-Ar-H), 7.76 (s, 2H; *p*-Ar-H), 4.94 (t, J = 7.8 Hz, 8H; C_9H_{19}-α), 2.54 (m, 8H; C_9H_{19}-β), 1.79 (m, 8H; C_9H_{19}-γ), 1.57 (s, 18H; *t*Bu), 1.52 (s, 18H; *t*Bu), 1.51 (s, 36H; *t*Bu), 0.79 ppm (t, J = 6.8 Hz, 12H; C_9H_{19}-Me); MS (MALDI-TOF): *m*/*z*: calcd for $C_{152}H_{184}N_{12}Zn_3$: 2375.4; found: 2374.4.

THa: Yield: 62%; ^{1}H NMR ($CDCl_3$): δ = 9.43 (d, J = 4.8 Hz, 4H; β-H), 9.33 (d, J = 4.9 Hz, 2H; β-H), 9.23 (d, J = 4.8 Hz, 4H; β-H), 9.17 (d, J = 5.0 Hz, 2H; β-H), 8.94 (d, J = 4.6 Hz, 4H; β-H), 8.83 (d, J = 4.8 Hz, 4H; β-H), 8.31 (d, J = 4.6 Hz, 2H; β-H), 8.29 (d, J = 4.9 Hz, 2H; β-H), 8.27 (d, J = 4.9 Hz, 2H; β-H), 8.18 (s, 2H; *o*-Ar-H), 8.15 (d, J = 8.0 Hz, 2H; *o*-Ar-H), 8.09 (d, J = 8.0 Hz, 2H; *o*-Ar-H), 8.01 (d, J = 8.0 Hz, 2H; β-H), 7.90 (d, J = 4.9 Hz, 2H; β-H), 7.66 (s, 1H; *p*-Ar-H), 7.31 (d, J = 7.8 Hz, 2H; *m*-Ar-H), 7.28 (d, J = 8.0 Hz, 2H, *m*-Ar-H), 7.22 (d, J = 8.7 Hz, 4H; *m*-Ar-H), 4.92 (brt, 8H; C_9H_{19}-α), 4.83 (brt, 4H; C_9H_{19}-α), 4.28 (t, J = 6.5 Hz, 4H; $C_{12}H_{25}$-α), 4.22 (t, J = 6.6 Hz, 2H; $C_{12}H_{25}$-α), 2.51 (m, 8H; C_9H_{19}-β), 2.41 (m, 4H; C_9H_{19}-β), 2.01 (m, 4H; $C_{12}H_{25}$-β), 1.96 (m, 2H; $C_{12}H_{25}$-β), −2.11 (s, 4H; NH), −2.27 ppm (s, 2H; NH) (*m*–Ar-H signals were obscured by the $CHCl_3$ peak); UV/Vis ($CHCl_3$): $\lambda_{max}(\varepsilon)$ = 659 (16100), 601 (33900), 566 (84800), 524 (92000), 472 (272000), 410 nm (296000 $M^{-1}cm^{-1}$); MS (MALDI-TOF): *m*/*z*: calcd for $C_{202}H_{260}N_{16}O_3Zn$: 3025.7; found: 3025.8.

TZa: Yield: quant; ^{1}H NMR ($CDCl_3$): δ = 9.56 (d, J = 4.9 Hz, 4H; β-H), 9.46 (d, J = 4.8 Hz, 2H; β-H), 9.38 (d, J = 4.8 Hz, 4H; β-H), 9.31 (d, J = 4.8 Hz, 2H; β-H), 9.05 (d, J = 4.6 Hz, 4H; β-H), 8.94 (d, J = 4.8 Hz, 2H; β-H), 8.85 (d, J = 4.8 Hz, 2H; β-H), 8.46 (d, J = 4.6 Hz, 4H; β-H), 8.44 (d, J = 5.0 Hz, 2H; β-H), 8.27 (d, J = 4.6 Hz, 4H; β-H), 8.20 (d, J = 1.6 Hz, 2H; *o*-Ar-H), 8.17 (dd, J = 8.1 Hz, J = 2.1 Hz, 2H; *o*-Ar-H), 8.10 (dd, J = 8.1 Hz, J = 2.2 Hz, 2H; *o*-Ar-H), 8.02 (d, J = 8.8 Hz, 2H; *o*-Ar-H), 7.90 (d, J = 5.0 Hz, 2H; β-H), 7.88 (d, J = 5.0 Hz, 2H; β-H), 7.66 (s, 1H; *p*-Ar-H), 7.32 (dd, J = 8.3 Hz, J = 2.6 Hz, 2H; *m*-Ar-H), 7.28 (dd, J = 8.2 Hz, J = 2.6 Hz, 2H; *m*-Ar-H), 7.22 (d, J = 8.9 Hz, 2H; *m*-Ar-H), 4.99 (t, J = 7.7 Hz, 8H; C_9H_{19}-α), 4.89 (t, J = 7.6 Hz, 4H; C_9H_{19}-α), 4.29 (t, J = 6.5 Hz, 4H; $C_{12}H_{25}$-α), 4.23 (t, J = 6.6 Hz, 2H; $C_{12}H_{25}$-α), 2.57 (m, 8H; C_9H_{19}-β), 2.47 (m, 4H; C_9H_{19}-β), 2.02 (m, 4H; $C_{12}H_{25}$-β), 1.96 (m, 2H; $C_{12}H_{25}$-β), 1.82 (m, 8H; C_9H_{19}-γ), 1.75 (m, 4H; C_9H_{19}-γ), 1.66 (m, 4H; $C_{12}H_{25}$-γ), 1.60 (m, 2H; $C_{12}H_{25}$-γ), 1.52 (s, 18H; *t*Bu), 0.91 (t, J = 6.9 Hz, 6H; $C_{12}H_{25}$-Me), 0.88 (t, J = 7.0 Hz, 3H; $C_{12}H_{25}$-Me), 0.81 (t, J = 7.0 Hz, 12H; C_9H_{19}-Me), 0.77 ppm (t, J = 7.0 Hz, 6H; C_9H_{19}-Me); UV/Vis ($CHCl_3$): $\lambda_{max}(\varepsilon)$ = 572 (75500), 475 (264000), 413 nm (294000 $M^{-1}cm^{-1}$); MS (MALDI-TOF): *m*/*z*: calcd for $C_{202}H_{254}N_{16}O_3Zn_4$: 3215.7; found: 3215.8.

THb: Yield: 20%; ^{1}H NMR ($CDCl_3$): δ = 9.44 (d, J = 4.6 Hz, 4H; β-H), 9.34 (d, J = 4.8 Hz, 2H; β-H), 9.25 (d, J = 4.6 Hz, 4H; β-H), 9.20 (d, J = 4.8 Hz, 2H; β-H), 8.95 (d, J = 4.6 Hz, 4H; β-H), 8.86 (d, 4.8 Hz, 2H; β-H), 8.84 (d, J = 4.8 Hz, 2H; β-H), 8.35 (d, J = 4.4 Hz, 4H; β-H), 8.33 (d, J = 4.8 Hz, 2H; β-H), 8.31 (d, J = 4.8 Hz, 2H; β-H), 8.20 (s, 2H; *o*-Ar-H), 8.11 (s, 2H; *o*-Ar-H), 8.06 (s, 2H; *o*-Ar-H), 7.98–7.97 (m, 4H; *o*-Ar-H and β-H), 7.96 (d, J = 4.8 Hz, 2H; β-H), 7.83 (t, J = 1.7 Hz, 2H; *p*-Ar-H), 7.76 (s, 1H; *p*-Ar-H), 7.68 (s, 1H; *p*-Ar-H), 4.94 (t, J = 7.0 Hz, 8H; C_9H_{19}-α), 4.85 (t, J = 7.1 Hz, 4H; C_9H_{19}-α), 2.54 (m, 8H; C_9H_{19}-β), 2.44 (m, 4H; C_9H_{19}-β), 1.79 (m, 8H; C_9H_{19}-γ), 1.72 (m, 4H; C_9H_{19}-γ), 1.59 (s, 18H; *t*Bu), 1.54 (s, 18H; *t*Bu), 1.49 (s, 18H; *t*Bu), 1.44 (s, 18H; *t*Bu), 0.82 (t, J = 6.9 Hz, C_9H_{19}-Me), 0.78 (t, J = 6.9 Hz, C_9H_{19}-Me), −2.07 (brs, 4H; NH), −2.22 ppm (brs, 2H; NH); MS (MALDI-TOF): *m*/*z*: calcd for $C_{190}H_{236}N_{16}Zn$: 2809.4; found: 2809.4.

TZb: Yield: quant; ^{1}H NMR ($CDCl_3$): δ = 9.58 (d, J = 4.6 Hz, 4H; β-H), 9.48 (d, J = 4.8 Hz, 2H; β-H), 9.39 (d, J = 4.8 Hz, 4H; β-H), 9.33 (d, J = 4.8 Hz, 2H; β-H), 9.06 (d, J = 4.6 Hz, 4H; β-H), 8.96 (d, J = 4.9 Hz, 2H; β-H), 8.87 (d, J = 4.9 Hz, 2H; β-H), 8.47 (d, J = 4.6 Hz, 4H; β-H), 8.46 (d, J = 4.8 Hz, 2H; β-H), 8.29 (d, J = 4.6 Hz, 2H; β-H), 8.22 (d, J = 1.6 Hz, 2H; *o*-Ar-H), 8.14 (t, J = 1.6 Hz, 2H; *o*-Ar-H), 8.07 (t, J = 1.6 Hz, 2H; *o*-Ar-H), 8.00 (d, J = 1.6 Hz, 2H; *o*-Ar-H), 7.92 (d, J = 4.8 Hz, 2H; β-H), 7.90 (d, J = 4.8 Hz, 2H; β-H), 7.83 (d, J = 1.6 Hz, 2H; *p*-Ar-H), 7.76 (d, J = 1.6 Hz, 2H; *p*-Ar-H), 7.67 (d, J = 1.6 Hz, 2H; *p*-Ar-H), 5.00 (t, J = 7.7 Hz, 8H; C_9H_{19}-α), 4.92 (t, J = 8.0 Hz, 4H; C_9H_{19}-α), 2.60 (m, 8H; C_9H_{19}-β), 2.50 (m, 4H; C_9H_{19}-β), 1.86 (m, 8H; C_9H_{19}-γ), 1.77 (m, 4H; C_9H_{19}-γ), 1.59 (s, 18H; *t*Bu), 1.55 (s, 18H; *t*Bu), 1.50 (s, 18H; *t*Bu), 1.44 (s, 18H; *t*Bu), 0.83 (t, J = 6.9 Hz, C_9H_{19}-Me), 0.79 ppm (t, J = 6.9 Hz, C_9H_{19}-Me); MS (MALDI-TOF): calcd for $C_{190}H_{230}N_{16}Zn_4$: 2999.6; found: 2999.2.

Typical procedure for DDQ/Sc(OTf)$_3$ oxidation reactions: The *meso*–*meso* linked oligomer, DDQ, and $Sc(OTf)_3$ in dry toluene[32] shielded from light were heated at 90 °C under an argon atmosphere. After cooling to room temperature, THF was added to the reaction mixture and the resulting solution was passed through an alumina column with THF as eluent. The solution obtained was evaporated to remove the solvent and the residue was recrystallized from CH_2Cl_2/CH_3CN.

FLZa: A mixture of **LZa** (21.5 mg, 8.5 μmol), DDQ (20 mg, 88 μmol), and $Sc(OTf)_3$ (40 mg, 82 μmol) in toluene (15 mL) shielded from light was heated at 90 °C for 3 h under an argon atmosphere. Yield: 19.1 mg, 7.6 μmol, 89%; ^{1}H NMR ([D$_5$]pyridine): δ = 8.67 (br, 2H), 8.62 (d, J = 4.1 Hz, 2H), 8.45 (br, 2H), 8.05 (d, J = 4.6 Hz, 2H), 8.01 (d, J = 4.13 Hz, 2H), 7.93 (d, J = 7.3 Hz, 4H), 7.87 (br, 6H), 7.37 (d, J = 8.3 Hz, 4H), 4.43 (br, 4H), 4.31 (t, J = 6.4 Hz, 4H), 2.75 (t, J = 6.8 Hz, 4H), 2.57 (m, 4H), 2.17 (m, 4H), 2.04 (m, 4H), 1.93 ppm (m, 4H) (several peaks were obscured by a large solvent signal); UV/Vis (toluene/5% *n*-butylamine): $\lambda_{max}(\varepsilon)$ = 499 (48600), 788 (25300), 1622 nm (9800 $M^{-1}cm^{-1}$); MS (MALDI-TOF): *m*/*z*: calcd for $C_{160}H_{192}N_{12}O_2Zn_3$: 2511.3; found: 2511.2.

FLZb: A mixture of **LZb** (8.1 mg, 3.4 μmol), DDQ (15 mg, 66 μmol), and $Sc(OTf)_3$ (30 mg, 61 μmol) in toluene (3 mL) shielded from light was heated at 90 °C for 3 h under an argon atmosphere. Yield: 6.1 mg, 2.6 μmol, 77%; ^{1}H NMR (CD_2Cl_2/1% *n*-butylamine (v/v)): δ = 8.24 (d, J = 4.6 Hz, 2H; β-H), 8.20 (s, 2H; β-H), 8.15 (d, J = 4.6 Hz, 2H; β-H),

7.76 (s, 2H; β-H), 7.64 (d, $J=4.4$ Hz, 2H; β-H), 7.63–7.61 (m, 8H; β-H, *o*-Ar-H, *p*-Ar-H), 7.56 (t, $J=1.9$ Hz, 2H; *p*-Ar-H), 7.43 (d, $J=1.9$ Hz, 4H; *o*-Ar-H), 6.73 (s, 2H; β-H), 6.71 (s, 2H; β-H), 4.05 (t, $J=8.3$ Hz, 4H; nonyl-α), 3.73 (t, $J=8.0$ Hz, 4H; nonyl-α), 2.24 (m, 4H; nonyl-β), 2.01 (m, 4H; nonyl-β), 1.44 (s, 36H; *t*Bu), 1.43 ppm (s, 36H; *t*Bu) (the other signals arising from the C_9H_{19} chain were obscured by signals from *n*-butylamine and could not be identified); MS (MALDI-TOF): *m*/*z*: calcd for $C_{152}H_{176}N_{12}Zn_3$: 2367.2; found: 2367.2.

FTZa: A mixture of **TZa** (16.3 mg, 5.1 μmol), DDQ (15 mg, 66 μmol), and $Sc(OTf)_3$ (30 mg, 61 μmol) in toluene (15 mL) shielded from light was heated at 90 °C for 2.5 h under an argon atmosphere. Yield: 13.9 mg, 4.3 μmol, 85%; UV/Vis (toluene/5% *n*-butylamine): $\lambda_{max}(\varepsilon)=418$ (103000), 584 (95700), 716 (102000), 1805 nm ($28100\,M^{-1}cm^{-1}$); MS (MALDI-TOF): *m*/*z*: calcd for $C_{202}H_{242}N1_6O_3Zn_4$: 3203.8; found: 3203.2.

FTZb: A mixture of **TZb** (9.1 mg, 3.0 μmol), DDQ (15 mg, 66 μmol), and $Sc(OTf)_3$ (30 mg, 61 μmol) in toluene (3 mL) shielded from light was heated at 90 °C for 3 h under an argon atmosphere. Yield: 6.8 mg, 2.3 μmol, 75%; MS (MALDI-TOF): *m*/*z*: calcd for $C_{190}H_{218}N_{16}Zn_4$ 2987.5; found: 2987.7.

Measurement of the two-photon absorption cross-section ($\sigma^{(2)}$): The TPA experiments were performed by using the open-aperture Z-scan method[53] with 130 fs pulses from an optical parametric amplifier (Light Conversion, TOPAS) operating at a 5 kHz repetition rate using a Ti:sapphire regenerative amplifier system (Spectra-Physics, Hurricane). The laser beam was divided into two and detected by two identical InGaAs photodiodes. One was monitored by an InGaAs PIN photodiode (New Focus) as a reference of the intensity, and the other was used for transmittance studies. After passing through an $f=10$ cm lens, the laser beam was focused and passed through a quartz cell. The position of the sample cell could be varied along the direction of the laser beam (z axis) and so the local power density within the sample cell could be changed under a constant laser power. The thickness of the cell was 1 mm. The laser beam transmitted from the sample cell was then probed by using the photodiode used for reference monitoring. The on-axis peak intensity of the incident pulses at the focal point I_0 ranged from 40 to 60 GW cm^{-1}. Assuming a Gaussian beam profile, the nonlinear absorption coefficient β can be obtained by curve-fitting to the observed open-aperture traces using Equation (1) in which α_0 is the linear absorption coefficient, l is the sample length, and z_0 is the diffraction length of the incident beam. After obtaining the nonlinear absorption coefficient β, the TPA cross-section $\sigma^{(2)}$ (given in units of $1\,GM=10^{-50}\,cm^4\,s\,photon^{-1}\,molecule^{-1}$) of a single solute molecule sample can be determined from Equation (2) in which N_A is the Avogadro constant, d is the concentration of the TPA compound in solution, h is Planck's constant, and ν is the frequency of the incident laser beam. To satisfy the condition $\alpha_0 l \ll 1$, which allows the pure TPA $\sigma^{(2)}$ values to be determined using a simulation procedure, the TPA cross-section value for AF-50 was measured as a reference compound; this control was found to exhibit a TPA value of 50 GM at 800 nm.

$$T(z) = 1 - \frac{\beta I_0 (1 - e^{-\alpha_0 l})}{2\alpha_0 [1 + (z/z_0)^2]}$$

$$\beta = \frac{\sigma^{(2)} N_A d \times 10^{-3}}{h\nu}$$

Acknowledgements

The work at Kyoto was partly supported by a Grant-in-Aid from the Ministry of Education, Culture, Sports, Science and Technology, Japan (No. 1920006). The work at Yonsei University was supported by the Star Faculty program from the Ministry of Education and Human Resources Development, Korea. S.Y.J., J.M.L., and K.S.K. acknowledge the BK21 fellowship. The authors thank Prof. Hiromitsu Maeda and Mr. Takashi Hashimoto, Ritsumeikan University, for MALDI-TOF MS measurements.

[1] S. Kawata, H.-B. Sun, T. Tanaka, K. Takada, *Nature* **2001**, *412*, 697.
[2] W. Zhou, S. M. Kuebler, K. L. Braun, T. Yu, J. K. Cammack, C. K. Ober, J. W. Perry, S. R. Marder, *Science* **2002**, *296*, 1106.
[3] D. A. Parthenopoulos, P. M. Rentzepis, *Science* **1989**, *245*, 843.
[4] B. H. Cumpston, S. P. Ananthavel, S. Barlow, D. L. Dyer, J. E. Ehrlich, L. L. Erskine, A. A. Heikal, S. M. Kuebler, I.-Y. S. Lee, D. McCord-Maughon, J. Qin, H. Röckel, M. Rumi, X.-L. Wu, S. R. Marder, J. W. Perry, *Nature* **1999**, *398*, 51.
[5] G. S. He, J. D. Bhawalkar, P. N. Prasad, B. A. Reinhardt, *Opt. Lett.* **1995**, *20*, 1524.
[6] J. E. Ehrlich, X. L. Wu, I.-Y. S. Lee, Z.-Y. Hu, H. Röckel, S. R. Marder, J. W. Perry, *Opt. Lett.* **1997**, *22*, 1843.
[7] J. D. Bhawalkar, N. D. Kumar, C.-F. Zhao, P. N. Prasad, *J. Clin. Laser Med. Surg.* **1997**, *15*, 201.
[8] A. Abbotto, L. Beverina, R. Bozio, A. Facchetti, C. Ferrante, G. A. Pagani, D. Pedron, R. Signorini, *Chem. Commun.* **2003**, 2144.
[9] a) M. Albota, D. Beljonne, J.-L. Brédas, J. E. Ehrlich, J.-Y. Fu, A. A. Heikal, S. E. Hess, T. Kogej, M. D. Levin, S. R. Marder, D. McCord-Maughon, J. W. Perry, H. Röckel, M. Rumi, G. Subramaniam, W. W. Webb, X.-L. Wu, C. Xu, *Science* **1998**, *281*, 1653; b) M. Rumi, J. E. Ehrlich, A. A. Heikal, J. W. Perry, S. Barlow, Z. Hu, D. McCord-Maughon, T. C. Parker, H. Roeckel, S. Thayumanavan, S. R. Marder, D. Beljonne, J.-L. Bredas, *J. Am. Chem. Soc.* **2000**, *122*, 9500.
[10] K. D. Belfield, Y. Liu, R. A. Negres, M. Fan, G. Pan, D. J. Hagan, F. E. Hernandez, *Chem. Mater.* **2002**, *14*, 3663.
[11] L. Cristian, I. Sasaki, P. G. Lacroix, B. Donnadieu, I. Asselberghs, K. Clays, A. C. Razus, *Chem. Mater.* **2004**, *16*, 3543.
[12] Y. Iwase, K. Kamada, K. Ohta, K. Kondo, *J. Mater. Chem.* **2003**, *13*, 1575.
[13] O.-K. Kim, K.-S. Lee, H. Y. Woo, K.-S. Kim, G. S. He, J. Swiatkiewicz, P. N. Prasad, *Chem. Mater.* **2000**, *12*, 284.
[14] F. Meng, B. Li, S. Qian, K. Chen, H. Tian, *Chem. Lett.* **2004**, *33*, 470.
[15] B. A. Reinhardt, L. L. Brott, S. J. Clarson, A. G. Dillard, J. C. Bhatt, R. Kannan, L. Yuan, G. S. He, P. N. Prasad, *Chem. Mater.* **1998**, *10*, 1863.
[16] L. Ventelon, S. Charier, L. Moreaux, J. Mertz, M. Blanchard-Desce, *Angew. Chem.* **2001**, *113*, 2156; *Angew. Chem. Int. Ed.* **2001**, *40*, 2098.
[17] J. Yoo, S. K. Yang, M.-Y. Jeong, H. C. Ahn, S.-J. Jeon, B. R. Cho, *Org. Lett.* **2003**, *5*, 645.
[18] K. S. Kim, S. B. Noh, T. Katsuda, S. Ito, A. Osuka, D. Kim, *Chem. Commun.* **2007**, 2479.
[19] a) G. P. Bartholomew, G. C. Bazan, *Acc. Chem. Res.* **2001**, *34*, 30; b) H. Y. Woo, J. W. Hong, B. Liu, A. Mikhailovsky, D. Korystov, G. C. Bazan, *J. Am. Chem. Soc.* **2005**, *127*, 820.
[20] a) O. Mongin, J. Brunel, L. Porrés, M. Blanchard-Desce, *Tetrahedron Lett.* **2003**, *44*, 2813; b) O. Mongin, T. R. Krishna, M. H. V. Werts, A.-M. Caminade, J.-P. Majoral, M. Blanchard-Desce, *Chem. Commun.* **2006**, 915.
[21] a) Y. Tanaka, S. Saito, S. Mori, N. Aratani, H. Shinokubo, N. Shibata, Y. Higuchi, Z. S. Yoon, K. S. Kim, S. B. Noh, J. K. Park, D. Kim, A. Osuka, *Angew. Chem.* **2008**, *120*, 624; *Angew. Chem. Int. Ed.* **2008**, *47*, 681; b) J. K. Park, Z. S. Yoon, M.-C. Yoon, K. S. Kim, S. Mori, J.-Y. Shin, A. Osuka, D. Kim, *J. Am. Chem. Soc.* **2008**, *130*, 1824; c) S. Mori, K. S. Kim, Z. S. Yoon, S. B. Noh, D. Kim, A. Osuka, *J. Am. Chem. Soc.* **2007**, *129*, 11344; d) Z. S. Yoon, J. H. Kwon, M.-C. Yoon, M. K. Koh, S. B. Noh, J. L. Sessler, J. T. Lee, D. Seidel, A. Aguilar, S. Shimizu, M. Suzuki, A. Osuka, D. Kim, *J. Am. Chem. Soc.* **2006**, *128*, 14128.
[22] B. R. Cho, S. B. Park, S. J. Lee, K. H. Son, S. H. Lee, M.-J. Lee, J. Yoo, Y. K. Lee, G. J. Lee, T. I. Kang, M. Cho, S.-J. Jeon, *J. Am. Chem. Soc.* **2001**, *123*, 6421.
[23] M. Drobizhev, A. Karotki, M. Kruk, A. Rebane, *Chem. Phys. Lett.* **2002**, *355*, 175.
[24] K. Kurotobi, K. S. Kim, S. B. Noh, D. Kim, A. Osuka, *Angew. Chem.* **2006**, *118*, 4048; *Angew. Chem. Int. Ed.* **2006**, *45*, 3944.

[25] T.-G. Zhang, Y. Zhao, I. Asselberghs, A. Persoons, K. Clays, M. J. Therien, *J. Am. Chem. Soc.* **2005**, *127*, 9710.
[26] M. Drobizhev, Y. Stepanenko, Y. Dzenis, A. Karotki, A. Rebane, P. N. Taylor, H. L. Anderson, *J. Am. Chem. Soc.* **2004**, *126*, 15352.
[27] M. Drobizhev, Y. Stepanenko, A. Rebane, C. J. Wilson, T. E. O. Screen, H. L. Anderson, *J. Am. Chem. Soc.* **2006**, *128*, 12432.
[28] I. Hisaki, S. Hiroto, K. S. Kim, S. B. Noh, D. Kim, H. Shinokubo, A. Osuka, *Angew. Chem.* **2007**, *119*, 5217; *Angew. Chem. Int. Ed.* **2007**, *46*, 5125.
[29] A. Karotki, M. Drobizhev, Y. Dzenis, P. N. Taylor, H. L. Anderson, A. Rebane, *Phys. Chem. Chem. Phys.* **2004**, *6*, 7.
[30] K. Ogawa, A. Ohashi, Y. Kobuke, K. Kamada, K. Ohta, *J. Am. Chem. Soc.* **2003**, *125*, 13356.
[31] T. E. O. Screen, J. R. G. Thorne, R. G. Denning, D. G. Bucknall, H. L. Anderson, *J. Am. Chem. Soc.* **2002**, *124*, 9712.
[32] a) A. Tsuda, A. Osuka, *Science* **2001**, *293*, 79; b) A. Tsuda, A. Osuka, *Adv. Mater.* **2002**, *14*, 75.
[33] D. Bonifazi, M. Scholl, F. Song, L. Echegoyen, G. Accorsi, N. Armaroli, F. Diederich, *Angew. Chem.* **2003**, *115*, 5116; *Angew. Chem. Int. Ed.* **2003**, *42*, 4966.
[34] a) H. Sato, K. Tashiro, H. Shinmori, A. Osuka, T. Aida, *Chem. Commun.* **2005**, 2324; b) H. Sato, K. Tashiro, H. Shinmori, A. Osuka, Y. Murata, K. Komatsu, T. Aida, *J. Am. Chem. Soc.* **2005**, *127*, 13086.
[35] A. Tsuda, Y. Nakamura, A. Osuka, *Chem. Commun.* **2003**, 1096.
[36] T. K. Ahn, K. S. Kim, D. Y. Kim, S. B. Noh, N. Aratani, C. Ikeda, A. Osuka, D. Kim, *J. Am. Chem. Soc.* **2006**, *128*, 1700.
[37] Y. Nakamura, N. Aratani, H. Shinokubo, A. Takagi, T. Kawai, T. Matsumoto, Z. S. Yoon, D. Y. Kim, T. K. Ahn, D. Kim, A. Muranaka, N. Kobayashi, A. Osuka, *J. Am. Chem. Soc.* **2006**, *128*, 4119.
[38] For a similar proposal and attempts to synthesize 2D extended Crossley-type conjugated porphyrin arrays, see: a) M. J. Crossley, L. J. Govenlock, J. K. Prashar, *J. Chem. Soc., Chem. Commun.* **1995**, 2379; b) J. R. Reimers, N. S. Huch, M. J. Crossley, *J. Porphyrins Phthalocyanines* **2002**, *6*, 795; c) T. Khoury, M. J. Crossley, *J. Porphyrins Phthalocyanines* **2004**, *8*, 725; d) T. Khoury, M. J. Crossley, *Chem. Commun.* **2007**, 4851.
[39] A *meso–meso* singly linked L-shaped trimer and T-shaped tetramer have already been synthesized by a classic acid-catalyzed condensation reaction as a result of scrambling byproducts.: S.-K. Hong, E. Jeoung, C.-H. Lee, *J. Porphyrins Phthalocyanines*, **2005**, *9*, 285.
[40] A. Osuka, H. Shimidzu, *Angew. Chem.* **1997**, *109*, 93; *Angew. Chem. Int. Ed. Engl.* **1997**, *36*, 135.
[41] N. Aratani, A. Takagi, Y. Yanagawa, T. Matsumoto, T. Kawai, Z. S. Yoon, D. Kim, A. Osuka, *Chem. Eur. J.* **2005**, *11*, 3389.
[42] N. Aratani, A. Osuka, *Chem. Rec.* **2003**, *3*, 225.
[43] S. Hiroto, A. Osuka, *J. Org. Chem.* **2005**, *70*, 4054.
[44] K. Sugiura, Y. Fujimoto, Y. Sakata, *Chem. Commun.* **2000**, 1105.
[45] C. Ryppa, M. O. Senge, S. S. Hatscher, E. Kleinpeter, P. Wacker, U. Schilde, A. Wiehe *Chem. Eur. J.* **2005**, *11*, 3427.
[46] a) J. S. Lindsey, I. C. Schreiman, H. C. Hsu, P. C. Kearney, A. M. Marguerettaz, *J. Org. Chem.* **1987**, *52*, 827; b) S. G. DiMagno, V. S.-Y. Lin, M. J. Therien, *J. Org. Chem.* **1993**, *58*, 5983.
[47] A. G. Hyslop, M. A. Kellett, P. M. Iovine, M. J. Therien, *J. Am. Chem. Soc.* **1998**, *120*, 12676.
[48] N. Aratani, A. Osuka, *Org. Lett.* **2001**, *3*, 4213.
[49] T. Ikeue, N. Aratani, A. Osuka, *Isr. J. Chem.* **2005**, *45*, 293.
[50] Y. Nakamura, N. Aratani, A. Osuka, *Chem. Asian J.* **2007**, *2*, 860.
[51] H. S. Cho, D. H. Jeong, S. Cho, D. Kim, Y. Matsuzaki, K. Tanaka, A. Tsuda, A. Osuka, *J. Am. Chem. Soc.* **2002**, *124*, 14642.
[52] Unfortunately, tuning of the two-photon excitation wavelength further into the IR region has been very difficult due to a limit of the IR OPA tuning range. In addition, the detection sensitivity of the InGaAs PIN photodiode was not high enough for TPA measurements further into the IR region.
[53] M. Sheik-Bahae, A. A. Said, T.-H. Wei, D. G. Hagan, E. W. van Stryland, *IEEE J. Quantum Electron.* **1990**, *26*, 760.

Received: April 24, 2008
Published online: July 30, 2008

